Research Article | Vol. 10, No. 2 | 1 Feb 2019 | BIOMEDICAL OPTICS EXPRESS 761
Biomedical Optics EXPRESS

Frequency analysis of oscillations in cerebral hemodynamics measured by time domain near infrared spectroscopy

MICHAL KACPRZAK,[1,*] PIOTR SAWOSZ,[1] WOJCIECH WEIGL,[2] DANIEL MILEJ,[1,3,4] ANNA GEREGA,[1] AND ADAM LIEBERT[1]

[1]*Nalecz Institute of Biocybernetics and Biomedical Engineering Polish Academy of Sciences Trojdena 4, 02-109 Warsaw, Poland*
[2]*Anesthesiology and Intensive Care, Department of Surgical Sciences, Uppsala University, Akademiska Hospital, 751 85 Uppsala, Sweden*
[3]*Department of Medical Biophysics, Western University, London, Ontario N6A 5C1, Canada*
[4]*Imaging Division, Lawson Health Research Institute, London, Ontario N6A 4V2, Canada*
**michal.kacprzak@ibib.waw.pl*

Abstract: In this paper, we propose the application of time-domain near-infrared spectroscopy to the assessment of oscillations in cerebral hemodynamics. These oscillations were observed in the statistical moments of the distributions of time of flight of photons (DTOFs) measured on the head. We analyzed the zeroth and second centralized moments of DTOFs (total number of photons and variance) to obtain their spectra to provide parameters for the frequency components of microcirculation, which differ between the extracerebral and intracerebral layers of the head. Analysis of these moments revealed statistically significant differences between a control group of healthy subjects and a group of patients with severe neurovascular disorders, which is a promising result for the assessment of cerebral microcirculation and cerebral autoregulation mechanisms.

1. Introduction

Rapid development of optical brain monitoring methods has occurred over the past two decades [1–4]. Near infrared spectroscopy (NIRS), a method based on the estimation of changes in oxy- and deoxyhemoglobin concentrations, has been used in numerous studies as an effective tool for oxygenation assessment during neurophysiological experiments [5]. Based on the noninvasive nature of NIRS, it is used for monitoring infants [6–8] or for long-term measurements on adult heads. This technique has also been applied in many studies on patients with severe neurological conditions caused by traumatic brain injuries (TBIs) [9–11] or strokes [12,13]. Furthermore, near infrared diffuse optics have been applied for perfusion assessment by tracking exogeneous dyes injected into veins [14]. Based on analysis of the kinetics of the inflow and outflow of the dye in the head structures, it has been reported that patients with severe neurovascular disorders are examined safely [15,16].

One novel approach to NIRS is time-domain NIRS (tdNIRS). In this modality, the distribution of times of flight of photons (DTOF) through tissue is obtained by using the time-correlated single photon counting technique [17–19]. The analysis of DTOFs on human heads provides depth-domain information regarding the tissue under investigation [20]. Additionally, changes in the optical properties and hemoglobin concentrations of the brain cortex are evaluated separately from extracerebral tissues [21–23].

Recently, several clinical applications of NIRS for the detection of oscillations in blood circulation and cerebral autoregulation assessment have been introduced [10,24–26]. Cerebral autoregulation is complex mechanism for maintain required level of cerebral blood flow (CBF) and preventing hypoperfusion and hyperperfusion in brain tissue. In primary studies it has been reported, that autoregulation mechanism stabilizes cerebral perfusion through a

#346892 https://doi.org/10.1364/BOE.10.000761
Journal © 2019 Received 27 Sep 2018; revised 23 Dec 2018; accepted 23 Dec 2018; published 23 Jan 2019

Biomedical Optics EXPRESS

mean arterial pressure (MAP) range of 60-150 mmHg [27]. However, this finding, cited and illustrated in numerous publications is corrected by recent studies. It has been shown, by the analysis of 41 studies in healthy humans, that slope in MAP vs. CBF above and below resting MAP was found to be 0.81 ± 0.77 in the hypotensive range and 0.21 ± 0.47 in the hypertensive range [28]. This indicates that the brain defends more effectively against hypertension than hypotension [29,30]. Moreover, the autoregulatory plateau of only ~10 mmHg was reported, when ABP oscillations were induced at 0.03 Hz [31]. The autoregulation mechanism operates similarly to a high-pass filter [28,32,33], where fast oscillations in heart rate (HR), respiration rate (RR), and sympathetically generated Mayer waves are transferred from arterial blood pressure (ABP) to intracranial pressure and CBF, whereas low-frequency (LF) perturbations ($f < 0.05$ Hz) are attenuated. For an impaired autoregulation mechanism, the cutoff frequency for the high-pass filter is decreased and the LF components are transferred to CBF. These findings were applied to the evaluation of autoregulation loss in patients [34,35]. However, for the reliable optical monitoring of these phenomena, the distinction between extra- and intracerebral oscillation is crucial. Therefore, in this study, we applied tdNIRS to the assessment of the filtering efficiency of spontaneous LF oscillations in cerebral hemodynamics by the autoregulation mechanism in afflicted patients and healthy subjects.

2. Methods

2.1 Instrumentation

The tdNIRS system developed for our measurements is presented in Fig. 1. This system uses picosecond laser sources and time-correlated single photon counting electronics (TCSPC) on the detection site. A laser driver (Sepia II, PicoQuant, Germany) and four semiconductor laser heads were adopted in the system to deliver laser pulses at 687 nm and 830 nm to both hemispheres of the head using separate light sources. This solution avoided the use of additional beam splitters or inter-fiber connections and facilitated the minimization of additional reflections, which are extremely undesirable in time-domain techniques, and maximization of the light power emitted into the tissue. Light pulses from each pair of 687- and 830-nm laser heads were delivered to the surface of the head by bifurcated 2-m step-index fibers with a diameter of 400 μm (Thorlabs, Sweden). Light pulses from both diodes were generated at a rate of 80 MHz and shifted between each wavelength at intervals of half of the repetition period by using different cable lengths. This temporal shift allowed us to analyze the DTOFs at both wavelengths within a single laser repetition period. The tips of the source fibers were arranged together with the tips of the detecting liquid light guides in two flexible fiber optic probes with a source-detector separation of 3 cm, which were located on both hemispheres of the head. The liquid light guides, which delivered diffusely reflected light to the detectors, were 2 m long and 4 mm in diameter, with NA = 0.48 (Newport, USA). For single photon detection, we used two high-speed hybrid photodetectors (HPM-100-50 Becker&Hickl, Germany). The power of the light delivered to the detectors was adjusted by neutral density filters located between the light guides and hybrid photodetectors and controlled by step motors. For the acquisition of the DTOFs, two PCI boards with TCSPC electronics (SPC-134, Becker&Hickl, Germany) were adopted. The recording of DTOFs during the experiments was triggered by a 10-Hz generator developed on the NI-DAQ 6221 board (National Instruments, USA). SPC-134 boards and an NI-DAQ 6221 controller were placed in a Magma PCI driver box (OSS, USA) and controlled by a laptop computer. To ensure stable measurement conditions, the system was subjected to a warm-up period of at least 45 min prior to each experiment. Instrumental response functions (IRFs) were measured immediately after each measurement by positioning the source fibers in front of the detection light guides with a sheet of white paper between them to fill the entire numerical aperture. The IRFs measured at both wavelengths for both detectors were no longer than 500 ps in full width at half maximum.

Biomedical Optics EXPRESS

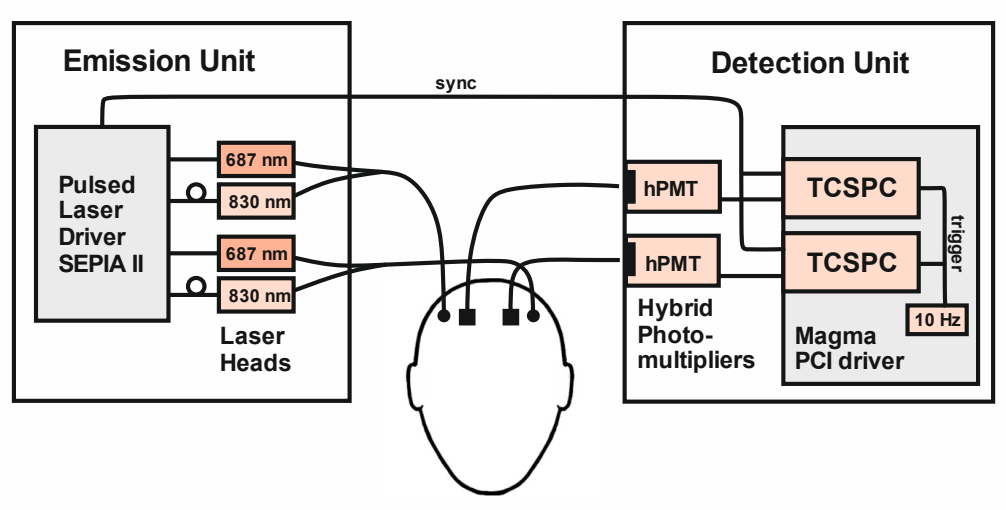

Fig. 1. Two-channel tdNIRS system equipped with four independent pulsed laser sources and two hybrid photomultipliers.

2.2. Data analysis

The DTOFs were acquired from two measurement channels with a sampling frequency of 10 Hz over 20 minutes of a resting state for healthy volunteers and 10 minutes for patients. The recorded time series of DTOFs were analyzed via calculation of their statistical moments, namely the total number of photons (N_{tot}), mean time of flight ($\langle t \rangle$), and variance in the DTOF (V). Based on different measurement conditions across a large group of volunteers and patients, the signals of the moments were normalized to the baseline of the mean signal from the first 30 s of measurements. This operation yielded the following information regarding changes in moments over time during the experiment: change of light attenuation $\Delta A = -log(N_{tot}/N_{tot0})$, mean time of flight $\Delta\langle t \rangle = \langle t \rangle - \langle t \rangle_0$, and variance $\Delta V = V - V_0$, where quantities with subscripts of zero indicate mean values from the first 30 s of measurements.

It has been reported in previous studies that higher moments of DTOFs, particularly variance, are highly sensitive to changes in the optical properties of deep tissue compartments under fiber optic probes, whereas changes in the zeroth moment (ΔA) reflect relatively superficial variations [21,22]. Considering these features, we calculated spectrograms of the ΔA and ΔV signals to derive information regarding the frequency components contained in both signals at both wavelengths. To calculate the amplitude spectra of ΔA and ΔV, fast Fourier transformation (FFT) calculations were performed in the Matlab R2017b environment. The spectra of ΔA and ΔV were parameterized by calculating mean values of the spectra for the low (0.005–0.1 Hz) and high (HF: 0.3–3 Hz) frequency ranges.

As outputs for this signal processing procedure, we introduced two factors, namely the attenuation autoregulation factor (AAF) and variance autoregulation factor (VAF). Both parameters are described as ratios between the LF and HF ranges of the spectra as follows: $AAF = P(\Delta A_{LF}) / P(\Delta A_{HF})$ and $VAF = P(\Delta V_{LF}) / P(\Delta V_{HF})$.

AAF and VAF were calculated separately in for groups of healthy subjects and patients and the statistical significance of the distributions of these factors was evaluated by a t-test.

2.3. In vivo experiments

Measurements on the healthy subjects were performed under clinical conditions with a group of 22 volunteers (mean age of 35 years, 15 males, 7 females) with no diagnosed neurological disorders.

Biomedical Optics EXPRESS

Ten adult patients (6 males, 4 females) from the intensive care unit (ICU) of a secondary care hospital in Warsaw were included in the experiment. The clinical characteristics and mechanisms of cerebral injury are listed in Table 1.

Table 1. Clinical data of patients included in the study

No.	Age	Sex	Primary mechanism of injury
1	47	M	TBI
2	38	M	Meningitis
3	50	M	TBI
4	54	F	TBI
5	63	M	TBI
6	52	F	Intracranial Hemorrhage
7	47	M	TBI
8	65	M	Cardiac Arrest
9	85	F	Stroke
10	83	F	Stroke

All patients included in the study had severe brain injuries with high risks of impaired autoregulation mechanisms, which qualified them for this study. The patients were monitored by standard medical equipment (i.e., measurement of SpO2 and ABP every 5 minutes). These measurements were not synchronized with the tdNIRS method but were used to ensure that patients maintained stable conditions during the measurements.

Our measurement protocol was approved by the Ethics Committee of the Medical University of Warsaw, Poland and carried out by following the principles of the Declaration of Helsinki and national law. The subjects and patients were monitored in a supine position for 20 minutes for healthy subjects and 10 minutes for patients with fiber optic probes fixed on the surface of the head below the hairline or over the motor cortex region at the C3/C4 points according to the 10/20 electroencephalography system. The laser power was limited to a level below the permissible maximum exposure for human tissue. Written informed consent was obtained from all healthy subjects and patients or the legally authorized representatives of patients.

Because of the complicated and heterogeneous nature of TBIs, where intracranial, extracerebral, and intracerebral edemas, hematomas, and contusions influence cerebral circulation [15], we decided not to distinguish between signals measured on healthy and afflicted hemispheres. All signals measured on both hemispheres at two wavelengths were simply compared to the control group directly.

3. Results

The signals acquired from the groups of healthy subjects and patients were analyzed by evaluating changes in the statistical moments of their DTOFs. Example time series of changes in light attenuation, mean time of flight, and variance of the DTOFs obtained from one of the healthy subjects is presented in Fig. 2. Because of the high sampling frequency, it is possible to observe oscillations in the signals originating from heart activity and respiration at both wavelengths used for measurement. These frequencies are clearly visible in the signal of light attenuation ΔA in Fig. 2(a). However, because of lower signal to noise ratios, they are barely visible in the signals of the higher order moments $\Delta\langle t\rangle$ and ΔV. It should be noted that for the 830 nm wavelength, amplitude oscillations in ΔA of nearly double the magnitude of those for the 687 nm wavelength were observed.

Biomedical Optics EXPRESS

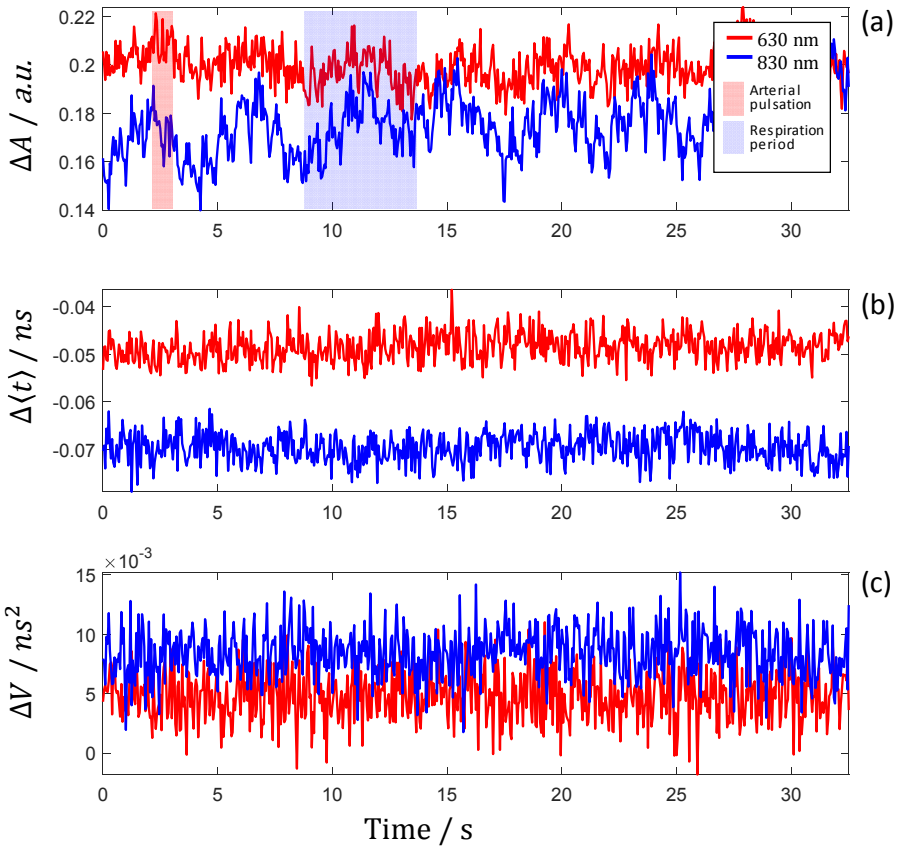

Fig. 2. Representative long-term recording of the changes in statistical moments of the DTOFs obtained during the measurement of a healthy subject at rest at two wavelengths: 687 and 830 nm. Frequency components related to heart rate and respiration are clearly visible in the light attenuation signal (a), but are not clear in the signals for change in the mean time of flight of photons (b) and variance of DTOF (c), where noise contamination is apparently higher.

Considering that the signals for change in the variance of DTOF ΔV should be much less contaminated by extracerebral hemodynamics, further analysis focused only on the signals of light attenuation change ΔA and variance of DTOF ΔV. The results of FFT analysis for the signals of ΔA and ΔV for a healthy subject are presented in Fig. 3.

These spectrograms were obtained at a wavelength of 830 nm for a male subject aged 38 years. In Fig. 3(a), peaks reflecting frequency components from the heart beating and respiration are clearly visible in the light attenuation signal ΔA. In the spectrum of the ΔV signal (Fig. 3(b)), these peaks are hidden below the noise level, but the arterial pulsation amplitude is visible. For variance, we observed a significant drop in the spectrum in the LF range (<0.1 Hz) compared to the same region in the ΔA spectrum.

Biomedical Optics EXPRESS

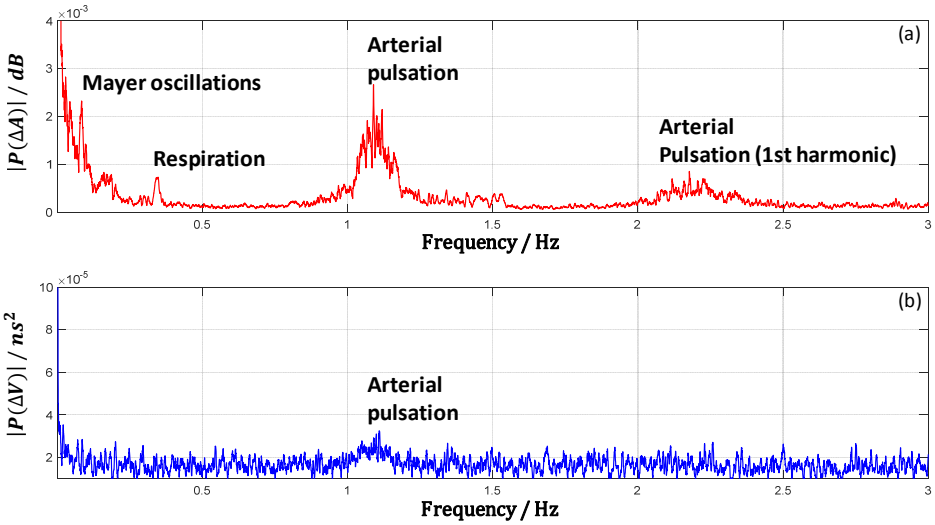

Fig. 3. Illustrative example of the amplitude spectrum analysis of the ΔA (a) and ΔV (b) signals for a healthy subject. In both graphs, the arterial pulsation components are visible, whereas the respiration arterial pulsation first harmonic and Mayer oscillations are only present in the ΔA (a) amplitude spectrum.

The results of power spectrum analysis for a representative TBI patient are presented in Fig. 4, where the spectra for a male aged 47 years are shown. In the ΔA spectrum, one can see peaks corresponding to heart rate and respiration located at approximately 1 and 0.3 Hz, respectively. In the spectrum of variance ΔV, a much higher level of noise is observed. Compared to the control group of healthy subjects, a significant elevation in the LF spectrum range is also be observed.

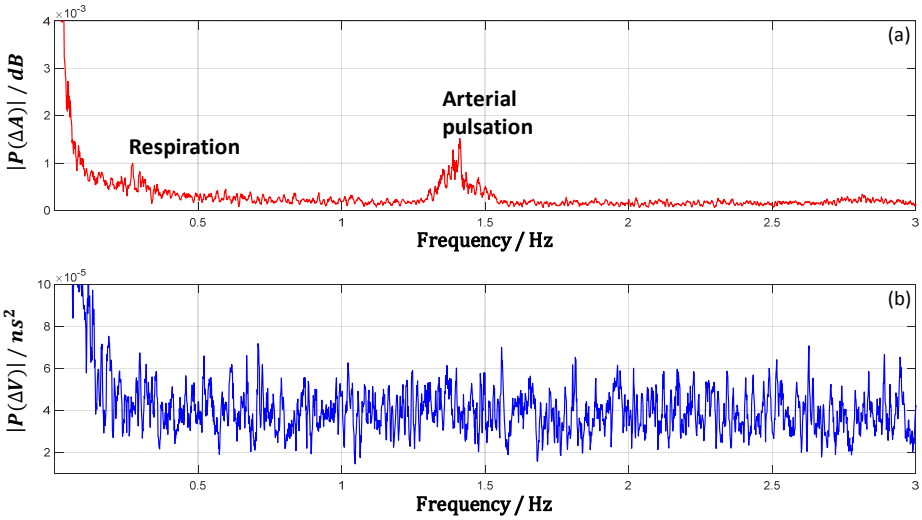

Fig. 4. Illustrative example of the amplitude spectrum analysis of the ΔA (a) and ΔV (b) signals for a TBI patient. In the ΔA signal (a), the arterial pulsation and respiration components are visible, whereas in the variance amplitude spectrum (b), all components are covered by noise, except for the LF components (f < 0.3 Hz).

To highlight the observed effects, we propose a parameterization procedure. We analyzed the spectra for the ΔA and ΔV signals in two regions: the LF range (0.005–0.1 Hz) and HF range (0.3–3 Hz). The spectra of both groups were averaged in these ranges for each healthy

Biomedical Optics EXPRESS

subject and patient. The results of statistical analysis on the obtained mean values are presented in Fig. 5.

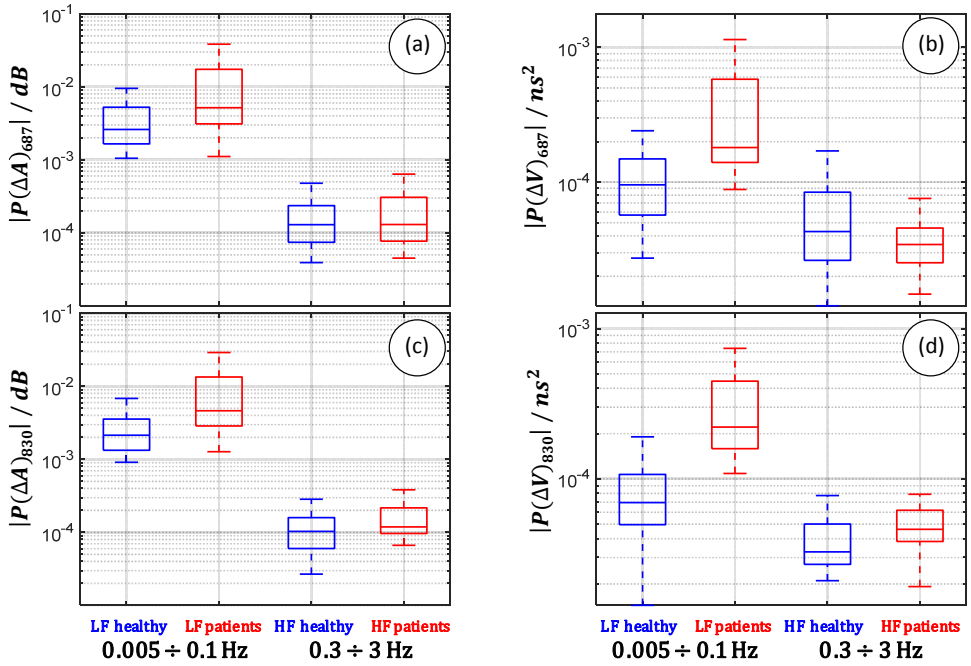

Fig. 5. Comparison of the amplitude spectra of the light attenuation signal (ΔA) (a and c) and variance (ΔV) (b and d) of DTOFs for LF (0.005–0.1 Hz) and HF (0.3 – 3 Hz) ranges for the group of healthy subjects and patients at wavelengths of 687 nm (a and b) and 830 nm (c and d). The boxes indicate the 25th and 75th percentiles of the distributions. The horizontal red lines inside the rectangles denote median values and the vertical bars reflect the maximum–minimum ranges.

In the healthy group, for light attenuation ΔA at both wavelengths in Figs. 5(a) and 5(c), the LF range had a higher amplitude than the HF range. For the wavelength of 687 nm, the mean level of the LF range was $1.5 \cdot 10^{-3}$ ns^2 and for the HF range, it reached $1 \cdot 10^{-4}$ ns^2. For the wavelength of 830 nm, the mean level of the LF range was $2 \cdot 10^{-3}$ ns^2 and for the HF range, it reached $1 \cdot 10^{-4}$ ns^2. In the variance graph in Figs. 5(b) and 5(d), the differences between LF and HF ranges were smaller for both wavelengths. For the wavelength of 687 nm, the mean level of the LF range was $9 \cdot 10^{-5}$ ns^2 and for the HF range, it reached $4 \cdot 10^{-5}$ ns^2. For the wavelength of 830 nm, the mean level of the LF range was $6.5 \cdot 10^{-5}$ ns^2 and for the HF range, it reached $3.2 \cdot 10^{-5}$ ns^2.

In the patient group, for the light attenuation ΔA at both wavelengths in Figs. 5(a) and 5(c), the LF range had a greater amplitude than the HF range. For the wavelength of 687 nm, the mean level of the LF range was $0.5 \cdot 10^{-3}$ ns^2 and for the HF range, it reached $1.0 \cdot 10^{-4}$ ns^2. For the wavelength of 830 nm, the mean level of the LF range in ΔA was $0.4 \cdot 10^{-3}$ ns^2 and for the HF range, it reached $1.0 \cdot 10^{-4}$ ns^2. In the variance ΔV graph in Fig. 5(b) and 5(d), the differences between the LF and HF ranges are also significant in compared to those of the healthy subjects. For the wavelength of 687 nm, the mean level of the LF range was $2.0 \cdot 10^{-4}$ ns^2 and for the HF range, it reached $3.5 \cdot 10^{-5}$ ns^2. For the wavelength of 830 nm, the mean level of the LF range was $3 \cdot 10^{-4}$ ns^2 and for the HF range, it reached $5.0 \cdot 10^{-5}$ ns^2.

Consequently, it was confirmed that the analysis of the light attenuation spectra obtained from both groups showed that the amplitudes of the LF components are significantly larger

Biomedical Optics EXPRESS

compared to those of the HF components. In the spectral analysis of variance, it was observed that the LF and HF ranges for the healthy group were similar level, whereas for the patient group, the LF range had an amplitude significantly than that of the HF range.

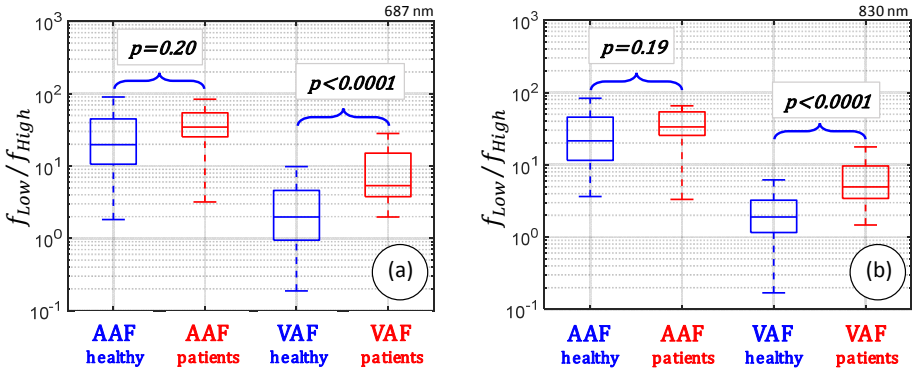

Fig. 6. AAF and VAF levels calculated for healthy subjects and patients with brain disorders at wavelengths of 687 nm (a) and 830 nm (b).

Regarding the assessment of LF and HF, we used the AAF and VAF parameters described in the methods section. The distribution of both parameters is presented in Fig. 6. There are no statistically significant differences between the healthy subjects and patient group in terms of the AAF parameter for both wavelengths ($p = 0.20$ and $p = 0.19$). For the VAF parameter, statistically significant differences between the healthy subjects and patient group were observed for both wavelengths ($p < 0.0001$).

4. Discussion and conclusions

According to the features of the moments described above, we decided to focus on the amplitude spectra of light attenuation and variance to assess oscillations in brain and systemic circulation. The spectra were calculated after long-term measurements of both the healthy subjects and patients. In Fig. 2, it was shown that basic oscillations (HR and RR) are observed in the pure signals of moments, especially in the attenuation signal (Fig. 2(a)) and spectra presented in Fig. 3(a), where Mayer oscillations and the first harmonic of arterial pulsation were also present. Because of high noise level, the latter oscillations are hidden in moments of higher order. However, through the acquisition of a large number of signal periods with a sampling frequency of 10 Hz, we were able to observe the HR in the spectra of variance for the healthy subject group (Fig. 3(b)). For the patients, the measurement duration was only half as long, and these frequencies were buried by the noise (Fig. 4(b)). Moreover, in contrast to the group of healthy subjects, we observed oscillations in the LF range in the spectra of variance (Fig. 4(b)) for the patients. This suggests that LF signals are present in the cerebral circulation of the patients. For the healthy subjects, this range was typically hidden in the spectra of ΔV (Fig. 3(b)) but present in the spectra of ΔA (Fig. 3(a)). Based on analysis of the oscillations in two different frequency ranges of 0.005–0.1 Hz and 0.3–3 Hz, we attempted to evaluate the autoregulation mechanism in both groups. In this study, we decided to analyze the statistical moments of DTOFs without further calculations to reveal the optical properties of tissues or other physiological parameters, such as changes in oxy- and deoxyhemoglobin concentrations, because the multiplication of a noisy signal amplifies the noise level and obscures the frequency components of the spectra.

Therefore, we determined that the autoregulation mechanism behaves like a high-pass filter, which blocks LF signals. In patients with severe brain disorders, this filtering effect could be disrupted. The tdNIRS system was applied to evaluate this effect. Statistical summaries of ΔA and ΔV for the LF and HF ranges at wavelengths of 687 nm and 830 nm for

Biomedical Optics EXPRESS

the healthy subjects and patient group are presented in Fig. 5. For the light attenuation signal, which is contaminated by extracerebral tissues, LF components is observed for both groups. For variance, the LF range was obscured in the control group and reached a similar amplitude compared to the HF range, whereas in the patient group ΔV spectra, the LF range amplitude was significantly higher than that of the HF range. This indicates that the cutoff frequency for brain autoregulation becomes much lower or disappears for patients with brain injuries. Therefore, we confirmed that spontaneous oscillations in LF spectra are transferred directly to the CBF. This effect can be employed in the assessment of cerebral autoregulation [32].

To quantify these phenomena, we introduced two parameters, namely AAF and VAF, as the ratios of the LF and HF ranges in their spectra. In Fig. 6, it is shown that VAF presents a statistically significant difference between the two groups, whereas AAF is similar between the groups.

In our study we included a group of patients with severe brain injuries. Only three patients were discharged to their homes and seven patients died. Based on such severe cases, the sensitivity of our method was confirmed, but it was not applied to less severe injuries or during recovery. In such situation, low frequencies <0.1 Hz in the variance signal could be partially blocked in patients and the statistical differences between the healthy subjects and patients could be negligible. Furthermore, the average age of the healthy subjects was significantly lower than the patients ($p< 0.0001$), which likely affected the results.

Although the patients included in the study all had severe brain injuries, the group was heterogeneous in terms of primary mechanism of injury (10 patients, 5 types of injuries), age (58 ± 15), and gender (4 females, 6 males). However, during the analysis of the spectra of the moments and comparisons of AAF and VAF between cases, no significant differences were observed. The LF and HF ranges, as well as the AAF and VAF, were randomly distributed around the mean values of the group and uncorrelated with patient condition, gender, or age. However, to prove correlations, the sample size for each type of injury should be larger.

Other mechanisms that affects the results of the analysis presented in this study include the occurrence of edema of the brain in some patients. This effect is represented in computed tomography imaging as the loss of sulci, compression of basilar cisterns, and flattening of ventricular margins [38]. In the presence of edema, oscillations originating from the HR or respiration could be completely blocked in cerebral circulation. This would lead to falsification of the VAF parameter for patients with edema and decrease the specificity of the proposed method.

In the light of other studies, approach presented in this paper focuses only on narrow effect of cerebral autoregulation, which is filtering of low oscillations in cerebral microcirculation. More complex study [36] allows for integration of many brain and systemic signals to determine this mechanism. Simultaneous measurements of intracranial pressure and arterial blood pressure together with the transcranial Doppler or optical signals allow for autoregulatory curve observations [32]. Moreover, this kind of measurements could optimize patients care by assessment of the cerebral perfusion pressure, which should be maintained in the specific range to protect the brain from both ischemia and hyperemic injury [24].

The tdNIRS technique was previously applied to cortex oxygenation assessment [37] and perfusion [38] successfully. Our present results demonstrate that tdNIRS used for the detection of autoregulatory deficiencies in patients with neurovascular disorders demonstrate significant final result. The frequency analysis of moments based on absolute units in Hz allows for comparative analysis of HR, RR, and other frequency components present in brain and systemic circulation for healthy subjects and patients. The tdNIRS technique combined with frequency analysis of the moments specially variance and VAF seems to be a promising tool for detecting deficits of cerebral autoregulation mechanisms.

Funding

National Science Centre, Poland (2011/03/D/ST7/02522, 2016/21/D/ST7/03454).

Biomedical Optics EXPRESS

Disclosures

The authors declare that there are no conflicts of interest related to this article.

References

1. T. Durduran and A. G. Yodh, "Diffuse correlation spectroscopy for non-invasive, micro-vascular cerebral blood flow measurement," Neuroimage **85**(Pt 1), 51–63 (2014).
2. A. Torricelli, D. Contini, A. Pifferi, M. Caffini, R. Re, L. Zucchelli, and L. Spinelli, "Time domain functional NIRS imaging for human brain mapping," Neuroimage **85**(Pt 1), 28–50 (2014).
3. W. Weigl, D. Milej, D. Janusek, S. Wojtkiewicz, P. Sawosz, M. Kacprzak, A. Gerega, R. Maniewski, and A. Liebert, "Application of optical methods in the monitoring of traumatic brain injury: A review," J. Cereb. Blood Flow Metab. **36**(11), 1825–1843 (2016).
4. R. Maniewski, A. Liebert, M. Kacprzak, and A. Zbiec, "Selected applications of near infrared optical methods in medical diagnosis," Opto-Electron. Rev. **12**, 255–262 (2004).
5. D. A. Boas, T. Gaudette, G. Strangman, X. Cheng, J. J. Marota, and J. B. Mandeville, "The accuracy of near infrared spectroscopy and imaging during focal changes in cerebral hemodynamics," Neuroimage **13**(1), 76–90 (2001).
6. L. Spinelli, L. Zucchelli, D. Contini, M. Caffini, J. Mehler, A. Fló, A. L. Ferry, L. Filippin, F. Macagno, L. Cattarossi, and A. Torricelli, "In vivo measure of neonate brain optical properties and hemodynamic parameters by time-domain near-infrared spectroscopy," Neurophotonics **4**(4), 041414 (2017).
7. S. L. Ferradal, K. Yuki, R. Vyas, C. G. Ha, F. Yi, C. Stopp, D. Wypij, H. H. Cheng, J. W. Newburger, A. K. Kaza, M. A. Franceschini, B. D. Kussman, and P. E. Grant, "Non-invasive Assessment of Cerebral Blood Flow and Oxygen Metabolism in Neonates during Hypothermic Cardiopulmonary Bypass: Feasibility and Clinical Implications," Sci Rep-Uk **7**, 44117 (2017).
8. G. Greisen, T. Leung, and M. Wolf, "Has the time come to use near-infrared spectroscopy as a routine clinical tool in preterm infants undergoing intensive care?" Philos Trans A Math Phys Eng Sci **369**(1955), 4440–4451 (2011).
9. C. Zweifel, G. Castellani, M. Czosnyka, A. Helmy, A. Manktelow, E. Carrera, K. M. Brady, P. J. Hutchinson, D. K. Menon, J. D. Pickard, and P. Smielewski, "Noninvasive monitoring of cerebrovascular reactivity with near infrared spectroscopy in head-injured patients," J. Neurotrauma **27**(11), 1951–1958 (2010).
10. D. Highton, A. Ghosh, I. Tachtsidis, J. Panovska-Griffiths, C. E. Elwell, and M. Smith, "Monitoring Cerebral Autoregulation After Brain Injury: Multimodal Assessment of Cerebral Slow-Wave Oscillations Using Near-Infrared Spectroscopy," Anesth. Analg. **121**(1), 198–205 (2015).
11. M. N. Kim, T. Durduran, S. Frangos, B. L. Edlow, E. M. Buckley, H. E. Moss, C. Zhou, G. Yu, R. Choe, E. Maloney-Wilensky, R. L. Wolf, M. S. Grady, J. H. Greenberg, J. M. Levine, A. G. Yodh, J. A. Detre, and W. A. Kofke, "Noninvasive measurement of cerebral blood flow and blood oxygenation using near-infrared and diffuse correlation spectroscopies in critically brain-injured adults," Neurocrit. Care **12**(2), 173–180 (2010).
12. P. Zirak, R. Delgado-Mederos, L. Dinia, D. Carrera, J. Martí-Fàbregas, and T. Durduran, "Transcranial diffuse optical monitoring of microvascular cerebral hemodynamics after thrombolysis in ischemic stroke," J. Biomed. Opt. **19**(1), 018002 (2014).
13. C. C. Lo, P. Y. Lin, Z. Y. Hoe, and J. J. J. Chen, "Near Infrared Spectroscopy Study of Cortical Excitability During Electrical Stimulation-Assisted Cycling for Neurorehabilitation of Stroke Patients," IEEE Trans. Neural Syst. Rehabil. Eng. **26**(6), 1292–1300 (2018).
14. C. Terborg, S. Bramer, S. Harscher, M. Simon, and O. W. Witte, "Bedside assessment of cerebral perfusion reductions in patients with acute ischaemic stroke by near-infrared spectroscopy and indocyanine green," J. Neurol. Neurosurg. Psychiatry **75**(1), 38–42 (2004).
15. W. Weigl, D. Milej, A. Gerega, B. Toczyłowska, P. Sawosz, M. Kacprzak, D. Janusek, S. Wojtkiewicz, R. Maniewski, and A. Liebert, "Confirmation of brain death using optical methods based on tracking of an optical contrast agent: assessment of diagnostic feasibility," Sci. Rep. **8**(1), 7332 (2018).
16. O. Steinkellner, C. Gruber, H. Wabnitz, A. Jelzow, J. Steinbrink, J. B. Fiebach, R. Macdonald, and H. Obrig, "Optical bedside monitoring of cerebral perfusion: technological and methodological advances applied in a study on acute ischemic stroke," J. Biomed. Opt. **15**(6), 061708 (2010).
17. H. Wabnitz, A. Jelzow, M. Mazurenka, O. Steinkellner, R. Macdonald, D. Milej, N. Żołek, M. Kacprzak, P. Sawosz, R. Maniewski, A. Liebert, S. Magazov, J. Hebden, F. Martelli, P. Di Ninni, G. Zaccanti, A. Torricelli, D. Contini, R. Re, L. Zucchelli, L. Spinelli, R. Cubeddu, and A. Pifferi, "Performance assessment of time-domain optical brain imagers, part 2: nEUROPt protocol," J. Biomed. Opt. **19**(8), 086012 (2014).
18. H. Wabnitz, D. R. Taubert, M. Mazurenka, O. Steinkellner, A. Jelzow, R. Macdonald, D. Milej, P. Sawosz, M. Kacprzak, A. Liebert, R. Cooper, J. Hebden, A. Pifferi, A. Farina, I. Bargigia, D. Contini, M. Caffini, L. Zucchelli, L. Spinelli, R. Cubeddu, and A. Torricelli, "Performance assessment of time-domain optical brain imagers, part 1: basic instrumental performance protocol," J. Biomed. Opt. **19**(8), 086010 (2014).
19. G. Giacalone, M. Zanoletti, D. Contini, R. Re, L. Spinelli, L. Roveri, and A. Torricelli, "Cerebral time domain-NIRS: reproducibility analysis, optical properties, hemoglobin species and tissue oxygen saturation in a cohort of adult subjects," Biomed. Opt. Express **8**(11), 4987–5000 (2017).

Biomedical Optics EXPRESS

20. P. Sawosz, M. Kacprzak, W. Weigl, A. Borowska-Solonynko, P. Krajewski, N. Zolek, B. Ciszek, R. Maniewski, and A. Liebert, "Experimental estimation of the photons visiting probability profiles in time-resolved diffuse reflectance measurement," Phys. Med. Biol. **57**(23), 7973–7981 (2012).
21. J. Steinbrink, H. Wabnitz, H. Obrig, A. Villringer, and H. Rinneberg, "Determining changes in NIR absorption using a layered model of the human head," Phys. Med. Biol. **46**(3), 879–896 (2001).
22. A. Liebert, H. Wabnitz, J. Steinbrink, H. Obrig, M. Möller, R. Macdonald, A. Villringer, and H. Rinneberg, "Time-resolved multidistance near-infrared spectroscopy of the adult head: intracerebral and extracerebral absorption changes from moments of distribution of times of flight of photons," Appl. Opt. **43**(15), 3037–3047 (2004).
23. A. Gerega, D. Milej, W. Weigl, M. Kacprzak, and A. Liebert, "Multiwavelength time-resolved near-infrared spectroscopy of the adult head: assessment of intracerebral and extracerebral absorption changes," Biomed. Opt. Express **9**(7), 2974–2993 (2018).
24. C. Zweifel, G. Castellani, M. Czosnyka, E. Carrera, K. M. Brady, P. J. Kirkpatrick, J. D. Pickard, and P. Smielewski, "Continuous assessment of cerebral autoregulation with near-infrared spectroscopy in adults after subarachnoid hemorrhage," Stroke **41**(9), 1963–1968 (2010).
25. C. Dias, M. J. Silva, E. Pereira, E. Monteiro, I. Maia, S. Barbosa, S. Silva, T. Honrado, A. Cerejo, M. J. H. Aries, P. Smielewski, J. A. Paiva, and M. Czosnyka, "Optimal Cerebral Perfusion Pressure Management at Bedside: A Single-Center Pilot Study," Neurocrit. Care **23**(1), 92–102 (2015).
26. J. Diedler, C. Zweifel, K. P. Budohoski, M. Kasprowicz, E. Sorrentino, C. Haubrich, K. M. Brady, M. Czosnyka, J. D. Pickard, and P. Smielewski, "The Limitations of Near-Infrared Spectroscopy to Assess Cerebrovascular Reactivity: the Role of Slow Frequency Oscillations," Anesth. Analg. **113**(4), 849–857 (2011).
27. N. A. Lassen, "Cerebral Blood Flow and Oxygen Consumption in Man," Physiol. Rev. **39**(2), 183–238 (1959).
28. C. K. Willie, Y. C. Tzeng, J. A. Fisher, and P. N. Ainslie, "Integrative regulation of human brain blood flow," J. Physiol. **592**(5), 841–859 (2014).
29. R. Aaslid, M. Blaha, G. Sviri, C. M. Douville, and D. W. Newell, "Asymmetric dynamic cerebral autoregulatory response to cyclic stimuli," Stroke **38**(5), 1465–1469 (2007).
30. B. Schmidt, J. Klingelhöfer, I. Perkes, and M. Czosnyka, "Cerebral Autoregulatory Response Depends on the Direction of Change in Perfusion Pressure," J. Neurotrauma **26**(5), 651–656 (2009).
31. C. O. Tan, "Defining the characteristic relationship between arterial pressure and cerebral flow," J. Appl. Physiol. **113**(8), 1194–1200 (2012).
32. J. Donnelly, K. P. Budohoski, P. Smielewski, and M. Czosnyka, "Regulation of the cerebral circulation: bedside assessment and clinical implications," Crit. Care **20**(1), 129 (2016).
33. C. A. Giller, "The Frequency-Dependent Behavior of Cerebral Autoregulation," Neurosurgery **27**(3), 362–368 (1990).
34. R. R. Diehl, D. Linden, D. Lücke, and P. Berlit, "Phase Relationship Between Cerebral Blood Flow Velocity and Blood Pressure. a Clinical Test of Autoregulation," Stroke **26**(10), 1801–1804 (1995).
35. C. Haubrich, W. Kruska, R. R. Diehl, W. Möller-Hartmann, and C. Klötzsch, "Dynamic autoregulation testing in patients with middle cerebral artery stenosis," Stroke **34**(8), 1881–1885 (2003).
36. M. Czosnyka, K. Brady, M. Reinhard, P. Smielewski, and L. A. Steiner, "Monitoring of cerebrovascular autoregulation: facts, myths, and missing links," Neurocrit. Care **10**(3), 373–386 (2009).
37. M. Kacprzak, A. Liebert, W. Staszkiewicz, A. Gabrusiewicz, P. Sawosz, G. Madycki, and R. Maniewski, "Application of a time-resolved optical brain imager for monitoring cerebral oxygenation during carotid surgery," J. Biomed. Opt. **17**(1), 016002 (2012).
38. O. Steinkellner, H. Wabnitz, A. Jelzow, R. Macdonald, C. Gruber, J. Steinbrink, and H. Obrig, "Cerebral Perfusion in Acute Stroke Monitored by Time-domain Near-infrared Reflectometry," Biocybern. Biomed. Eng. **32**(1), 3–16 (2012).